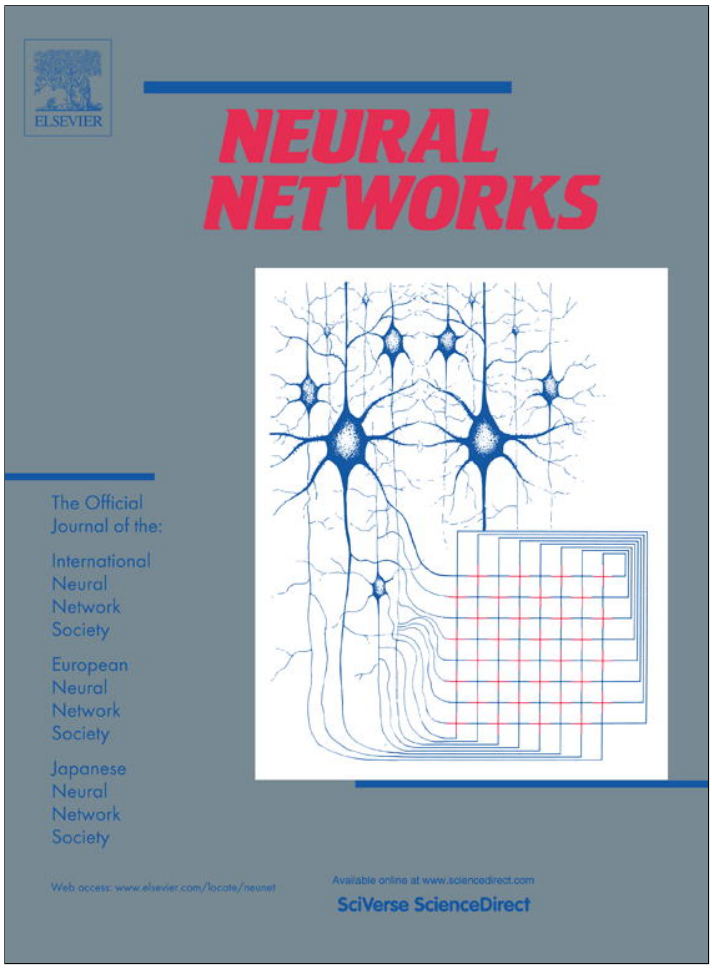

Neural Networks 46 (2013) 249–259

Contents lists available at SciVerse ScienceDirect

Neural Networks

journal homepage: www.elsevier.com/locate/neunet

Effects of spike sorting error on the Granger causality index

Pei-Chiang Shao [a], Wan-Ting Tseng [b], Chung-Chih Kuo [c], Wei-Chang Shann [a], Meng-Li Tsai [d], Chien-Chang Yen [e,*]

[a] Department of Mathematics, National Central University, Jhongli 32001, Taiwan
[b] Institute of Zoology, National Taiwan University, Taipei 10617, Taiwan
[c] Department of Physiology, School of Medicine, College of Medicine, Tzu Chi University, Hualien 97004, Taiwan
[d] Department of Biomechatronic Engineering, National Ilan University, Ilan 26047, Taiwan
[e] Department of Mathematics, Fu-Jen Catholic University, Xinzhuang 24205, Taiwan

ARTICLE INFO

Article history:
Received 8 January 2013
Received in revised form 21 May 2013
Accepted 4 June 2013

Keywords:
Granger causality index
Spike sorting
Vector autoregressive model

ABSTRACT

Accurately sorting individual neurons is a technical challenge and plays an important role in identifying information flow among neurons. Spike sorting errors are almost unavoidable and can roughly be divided into two types: false positives (FPs) and false negatives (FNs). This study investigates how FPs and FNs affect results of the Granger causality (GC) analysis, a powerful method for detecting causal interactions between time series signals. We derived an explicit formula based on a first order vector autoregressive model to analytically study the effects of FPs and FNs. The proposed formula was able to reveal the intrinsic properties of the GC, and was verified by simulation studies. The effects of FPs and FNs were further evaluated using real experimental data from the ventroposterior medial nucleus of the thalamus. Some practical suggestions for spike sorting are also provided in this paper.

1. Introduction

In neuroscience research, it is important to identify information flow among multiple neurons in the brain, according to the recorded neural activity data. A powerful method for achieving this is the Granger causality (GC) which arose in economics after being introduced by Wiener and Granger (Granger, 1969, 1980; Wiener, 1956). The GC is a time series inference (TSI) type of method, proposes that if the prediction of one time series can be improved with the knowledge of a second time series, then there is a causal influence from the second time series to the first. This prediction is made by using the vector autoregressive (VAR) model. In this model, if the variance of the prediction error of one time series at the present time can be reduced by including the past values of another series, then the latter is said to Granger-cause the former. This causality can be quantified by the so-called GC Index (GCI) which can be used to determine whether there is any causal interaction between time series. The GC was shown to be effective and has been widely deployed in recent neuroscience research (Bressler, Richter, Chen, & Ding, 2007; Cadotte, DeMarse, He, & Ding, 2008; Cadotte et al., 2010; Cao, Maran, Dhamala, Jaeger, & Heck, 2012; Zhang et al., 2012). In addition to the time domain GC, other versions of the GC (e.g., frequency, and time–frequency domain) have been developed as well (Baccala & Sameshima, 2001; Dhamala, Rangarajan, & Ding, 2008). The time domain formulation of GCI is briefly introduced in the next section, and we refer the reader to an article by Bressler and Seth (2011) for more details about the GC.

Neurons emit action potentials (APs) that are known as *spikes* and play an important role in communicating among cells. The temporal sequence of APs produced by a neuron, which shows its own activity, is also known as a *spike train*. In multi-channel recordings (Brown, Kass, & Mitra, 2004), the APS of neurons are detected and differentiated from background electrical noise before single-unit spike trains are used to probe neural behaviors. This technical procedure is called *spike sorting*. However, it is not easy to obtain spike train data that fully agree with the AP because of noise, superimposed APs, and difficulties of differentiating waveforms of APs from different neurons. Spike sorting often introduces unavoidable errors (Deborah, Won, & Patrick, 2003; Lewicki, 1998). These errors can roughly be divided into two types, false positives (FPs) and false negatives (FNs). An FP means an error detection of an event that is not a real spike (just an electrical noise) or is a spike from another neuron. Conversely, an FN means that real spikes were not detected or were classified into groups of other neurons. One may be interested in the question: "How do FPs and FNs affect the estimation of functional connectivity among neurons?". This study answered this question analytically and also via numerical simulations. The change in the GCI due to spike sorting errors was derived analytically to form an explicit formula,

* Corresponding author. Tel.: +886 2 2905 3547.
E-mail address: yen@math.fju.edu.tw (C.-C. Yen).

0893-6080/$ – see front matter © 2013 Elsevier Ltd. All rights reserved.
http://dx.doi.org/10.1016/j.neunet.2013.06.001

and a direct discussion of the effects of FPs and FNs is possible. Moreover, numerical simulations were used to verify the analyses. We constructed three types of models for sorting errors: those with uniform, random, and concentrative distributions. That is, errors occur uniformly, randomly, and concentratively in spike trains. Changes in the GCI were computed as these types of spike sorting errors were artificially added to the simulated spike trains, and the effects on the directional interactions were also investigated.

Finally, it is worth noting that spike trains are non-equally spaced data and are regarded as a point process. Interpolation or filtering is usually employed to convert point processes to equally spaced time series. Previous studies on spike trains (Kaminski, Ding, Truccolo, & Bressler, 2001; Zhu, Lai, Hoppensteadt, & He, 2003) proposed several methods to convert a time series from being non-equally spaced to equally spaced. This study adopted the procedure of binning to convert spike trains into time series data, which are suitable for GC analyses. Although the GCI between two point processes has been directly defined in Kim, Putrino, Ghosh, and Brown (2011) recently, we still cannot abandon binning because it reduces the complexity of analysis, and considers also the effect of temporal summation of action potentials in the neuroscience.

This article is organized as follows. Section 2 presents an analytic formula based on a first order autoregression to show how error processes affect the GCI. Section 3 presents some models for sorting errors and probes the proposed formula further via numerical simulations. Section 4 presents a real data evaluation where the effects of sorting error on the GCI are evaluated using real experimental data. Section 5 provides some suggestions for spike sorting and the discussion.

2. Modeling and analysis

Based on a first order autoregression, we derived an explicit formula for changes in the GCI in terms of four parameters involving the error process. We also investigated the influences of various types of errors on the GCI indicated by the proposed formula.

2.1. A short introduction to the GCI

Let x and y be two stationary time series with zero means. The first order linear autoregressive model for x and y is given by

$$\begin{bmatrix} x(n) \\ y(n) \end{bmatrix} = \mathbf{A} \begin{bmatrix} x(n-1) \\ y(n-1) \end{bmatrix} + \begin{bmatrix} \epsilon(n) \\ \eta(n) \end{bmatrix}, \tag{1}$$

where $\mathbf{A}$ is the model coefficient matrix, and the residuals ϵ and η are zero-mean uncorrelated white noises with covariance matrix $\mathbf{\Sigma}$. Here the variances $\mathrm{Var}(\epsilon)$ and $\mathrm{Var}(\eta)$ are called prediction errors, which measure the accuracy of the autoregressive prediction. More specifically, $\mathrm{Var}(\eta)$ measures the accuracy of the prediction of $y(n)$ based on the previous values $x(n-1)$ and $y(n-1)$.

Now consider the reduced model that excludes the time series variable x

$$y(n) = B\, y(n-1) + \zeta(n), \tag{2}$$

where B is the corresponding model coefficient. The variance $\mathrm{Var}(\zeta)$ measures the accuracy of the prediction of $y(n)$ based only on its previous value $y(n-1)$. For η in (1) and ζ in (2), if $\mathrm{Var}(\eta)$ is significantly less than $\mathrm{Var}(\zeta)$ in some statistical sense, then we say that x Granger-cause y. This causality can be quantified by the GCI from x to y formulated as:

$$F_{x\to y} = \ln \frac{\mathrm{Var}(\zeta)}{\mathrm{Var}(\eta)}. \tag{3}$$

It is clear that $F_{x\to y} = 0$ when $\mathrm{Var}(\eta) = \mathrm{Var}(\zeta)$, i.e., x has no causal influence on y, and $F_{x\to y} > 0$ when x Granger-cause y. Notice that $F_{x\to y}$ is nonnegative, i.e., $\mathrm{Var}(\eta)$ is bounded above by $\mathrm{Var}(\zeta)$, since the full model defined in (1) should have a better prediction ability than the reduced model defined in (2). Finally, we note that the GCI values should be checked for significance by using hypothesis testing, and more details of the GCI can be found in Ding, Chen, and Bressler (2006), Granger (1969, 1980).

2.2. An explicit formula

When inaccurate spike sorting occurs, the sorting errors can be regarded as a perturbed error process. For simplicity, we assume that only the source process x has a sorting error and the corresponding error process is denoted by δx. We can assume that δx is zero mean and the model in (1) is perturbed as follows when δx is superposed on x:

$$\begin{bmatrix} \{x+\delta x\}(n) \\ y(n) \end{bmatrix} = \tilde{\mathbf{A}} \begin{bmatrix} \{x+\delta x\}(n-1) \\ y(n-1) \end{bmatrix} + \begin{bmatrix} \tilde{\epsilon}(n) \\ \tilde{\eta}(n) \end{bmatrix}, \tag{4}$$

where $\tilde{\mathbf{A}}$ is the corresponding model coefficient matrix, and the residuals $\tilde{\epsilon}$ and $\tilde{\eta}$ have the covariance matrix $\tilde{\mathbf{\Sigma}}$. Let $S_y := \mathrm{Var}(\zeta)$, $S := \mathrm{Var}(\eta)$, and $\tilde{S} := \mathrm{Var}(\tilde{\eta})$. Since the perturbed quantity δx is superposed only on x, the reduced models for (1) and (4) are the same as (2). Then the original GCI from x to y and the perturbed GCI from $x+\delta x$ to y are

$$F = \ln \frac{S_y}{S} \quad \text{and} \quad \tilde{F} = \ln \frac{S_y}{\tilde{S}}, \tag{5}$$

respectively. To investigate the perturbed GCI, we derived an explicit formula for $\tilde{F}$ in terms of four parameters involving δx which are $\xi_1 := E(\delta x_1^2)$, $\xi_2 := E(x_1 \delta x_1)$, $\xi_3 := E(y_2 \delta x_1)$, and $\xi_4 := E(y_1 \delta x_1)$. Further denote $X_0 = E(x_1^2)$, $Y_0 = E(y_1^2)$, $Y_1 = E(y_1 y_2)$, $Z_1 = E(x_1 y_1)$, and $Z_2 = E(x_1 y_2)$. We are now ready to present the formula for $\tilde{F}$.

Proposition 1. *In the situation described above, $\tilde{F}$ can be presented explicitly by the following formula (for calculation see the Appendix):*

$$\tilde{F} = \ln \frac{S_y}{S+\Theta}, \quad \Theta = (S_y - S)I, \tag{6}$$

where

$$\begin{aligned} I = {} & \frac{1}{Y_0(X_0+\xi_1+2\xi_2) - (\xi_4+Z_1)^2} \Big\{ Y_0(X_0+\xi_1+2\xi_2) \\ & - \frac{1}{S_y - S}\big[Y_0(\xi_3+Z_2)^2 + (Y_0 - S)(\xi_4+Z_1)^2 \\ & - 2Y_1(\xi_3+Z_2)(\xi_4+Z_1)\big] \Big\}. \end{aligned} \tag{7}$$

Note that since $S+\Theta$ in (6) is bounded above by S_y, we have that Θ is upper bounded by $S_y - S$, i.e., I has an upper bound 1.

We end this subsection by the following two remarks.

Remark 1. In the same situation of Proposition 1, the following inequalities hold:

$$Y_0 \geq S_y \geq S \quad \text{and} \quad Y_1 \leq 0. \tag{8}$$

According to (2), we have $Y_0 = \mathrm{Var}(y_1) \geq \mathrm{Var}(\zeta) = S_y$. The remainder $S_y \geq S$ just follows by the reason that the prediction error of the reduced model in (4) is always less than or equal to that of the full model in (1). The latter holds because of the stationary assumption. If $Y_1 = E(y_1 y_2) > 0$, then y will not be stationary. Thus $Y_1 \leq 0$.

Remark 2. The following result can be obtained easily by using (5) and (6).

$$\begin{aligned} &\tilde{F} > F, \quad \text{if } I < 0. \\ &\tilde{F} = F, \quad \text{if } I = 0. \\ &\tilde{F} < F, \quad \text{if } 0 < I < 1. \\ &\tilde{F} = 0, \quad \text{if } I = 1. \end{aligned} \tag{9}$$

2.3. Essential GCI factors

The formula defined by (6) and (7) is complicated but it reveals the intrinsic property of the perturbed GCI, depending on the four factors ξ_1, ξ_2, ξ_3 and ξ_4 which, by the definition, capture the main properties of error signals, namely, the spike sorting errors. A systematic characterization of these parameters' influences on the GCI would provide a heuristic understanding of the effect of spike sorting error for researchers to make further decisions. Thus, in this subsection we discuss Proposition 1 more by a total of five different situations and relate each of them to a biological meaning.

We now present the following corollaries for investigating the term I defined in (7), and this is equivalent to investigating the term $\tilde{F}$ in (6).

Corollary 1 ($\xi_2 = \xi_3 = \xi_4 = 0$)**.** *We start with the simple case in which the error process δx is uncorrelated with the underlying processes x and y, i.e., $\xi_2 = \xi_3 = \xi_4 = 0$. In this case I can be simplified as follows:*

$$I(\xi_1) = \frac{Y_0\xi_1}{Y_0\xi_1 + [X_0Y_0 - Z_1^2]}. \tag{10}$$

The above equation shows that I increases as ξ_1 increases, but it is bounded above by the limit $L := \lim_{\xi_1\to\infty} I(\xi_1) = 1$. Hence, by (6), the weakened GCI $\tilde{F}$ is bounded below by $\lim_{\xi_1\to\infty} \tilde{F}(\xi_1) = \ln \frac{S_y}{S+(S_y-S)L} = \ln \frac{S_y}{S_y} = 0$. In reality, this limit cannot be attained because the variance $\xi_1 = E(\delta x_1^2)$ cannot approach infinity. Thus, the GCI will never vanish if the error process δx is uncorrelated with the underlying process x. We refer to this corollary as FPs being composed of electrical noises or the spikes of other unconnected neurons during spike sorting.

Corollary 2 ($\xi_2 < 0, \xi_3 < 0, \xi_4 < 0$)**.** *Suppose the error process δx is negatively correlated with the underlying processes x and y, i.e., ξ_2, ξ_3, and ξ_4 are all negative. Since the perturbed quantity δx is considered to be produced from inaccurate spike sorting, the maximal negative quantity which δx can be is $-x$. Therefore, we have the following constraint:*

$$-X_0 \le \xi_2 < 0, \qquad -Z_2 \le \xi_3 < 0, \qquad -Z_1 \le \xi_4 < 0, \tag{11}$$

and the equalities are attained when $\delta x = -x$.

Now, according to (7), (8) and (11), I is positive, increasing, and bounded above by 1. In other words, $\Theta \to S_y - S$ and $\tilde{F} \to 0$ as $\xi_1 \to \infty$ or $(\xi_2, \xi_3, \xi_4) \to (-X_0, -Z_2, -Z_1)$. This corollary is related to FNs in spike sorting.

Corollary 3 ($\xi_2 < 0, \xi_3 < 0, \xi_4 < 0$ *Simplified*)**.** *Suppose δx is correlated with the underlying processes as in Corollary 2. If y is further completely induced by x, i.e., y cannot explain itself ($B = 0$ in (2)), then we obtain $S_y = Y_0$, $Y_1 = 0$ and (7) can be further simplified as:*

$$I = \frac{Y_0(X_0 + \xi_1 + 2\xi_2) - (\xi_4 + Z_1)^2 - \frac{Y_0}{S_y - S}(\xi_3 + Z_2)^2}{Y_0(X_0 + \xi_1 + 2\xi_2) - (\xi_4 + Z_1)^2}. \tag{12}$$

Eq. (12) still shows us that $I \to 1$ as $\xi_1 \to \infty$. On the other hand, if ξ_1 is fixed and the negative correlation between x and δx increases (i.e., (ξ_2, ξ_3, ξ_4) decreases simultaneously to $(-X_0, -Z_2, -Z_1)$), then the value I increases to 1 because of the quadratic convergence:

$$(\xi_3 + Z_2)^2 \to 0. \tag{13}$$

Note that when (ξ_2, ξ_3, ξ_4) attains the lower bound $(-X_0, -Z_2, -Z_1)$, i.e., $\delta x = -x$, there is nothing left to analyze. Therefore, we do not consider this case.

Corollary 4 ($\xi_2 = 0, \xi_3 > 0, \xi_4 > 0$)**.** *Suppose the error process δx is positively correlated with y, and is uncorrelated with x, i.e., $\xi_2 = 0, \xi_3 > 0$, and $\xi_4 > 0$. Since $I = 0$ when $\xi_1 = \xi_2 = \xi_3 = \xi_4 = 0$, it is easy to conclude that, in this case, I is negative and decreasing, i.e., $\tilde{F} > F$ and $\tilde{F}$ increases as ξ_3 or ξ_4 increase. We refer to this corollary as FPs being composed of spikes of some connected neurons which are positively correlated with the target neuron during spike sorting.*

Corollary 5 ($\xi_2 > 0, \xi_3 > 0, \xi_4 > 0$)**.** *Suppose the error process δx is positively correlated with both x and y, i.e., $\xi_2 > 0, \xi_3 > 0$, and $\xi_4 > 0$. Since I is increasing in ξ_2, we know that $\tilde{F}$ is then decreasing in ξ_2. Therefore, $\tilde{F}$ in this case exhibits the same behavior as that in Corollary 4 if (ξ_3, ξ_4) dominates ξ_2; but $\tilde{F}$ is decreasing if ξ_2 dominates (ξ_3, ξ_4). We refer to this corollary as FPs being composed of spikes of some connected neurons which are positively correlated with both of source and target neurons during spike sorting.*

The results of above five corollaries are schematically summarized in Table 1.

2.4. GCI vs. variance reduction

Because $0 \le S \le S_y$, we set $S = (1-k)S_y$ with $0 \le k \le 1$ and the GCI in (5) becomes

$$F = \ln \frac{S_y}{(1-k)S_y} = -\ln(1-k). \tag{14}$$

Next, relate F and k through $k = 1 - \exp(-F)$. Since $S_y - S = kS_y$, $k = (S_y - S)/S_y$ represents the percentage of variance reduction. More precisely, it represents the relative decrease in prediction errors from the reduced model (2) to the full model (1). For example, $k = 0$ means no (0%) variance reduction, and the GCI is equal to zero. On the contrary, $k = 1$ means a total (100%) variance reduction, and the GCI is equal to infinity. Fig. 1 shows how the GCI relates to k, and it is almost totally reduced when the GCI is equal to 5.

3. Simulation study

Here, we present some models for sorting errors and further probe formula (7) via numerical simulations. For the FP case, we first consider that FPs are made up of electrical noises or spikes of unconnected neurons. Spikes of connected neurons are considered in Section 3.4.

3.1. Models

We first construct a point process $X = \{p_1, p_2, \ldots, p_N\}$ generated by a Poisson process with rate λ in the time interval $[0, T]$, where N is the total number of points. The second point process $Y = \{q_1, q_2, \ldots, q_N\}$ is then generated by $Y = X + \mathcal{N}(m, \sigma)$, where $\mathcal{N}(m, \sigma)$ is a normal random variable with mean m and standard deviation σ. More precisely, $q_i = p_i + \mathcal{N}(m, \sigma)$, $i = 1, \ldots, N$. The point process Y presents a time lag m with respect to X if $m > 0$ and $\sigma = 0$. This study only considers $m > 0$ and $\sigma > 0$.

Table 1
A schematic summary of Corollaries 1–5. The factors ξ_i, $i = 1, 2, 3, 4$ and error process δx are described in Section 2.2. $+$ ($-$) stands for positive (negative) sign. FP (FN) stands for false positive (negative). $\uparrow$ ($\downarrow$) stands for increasing (decreasing).

ξ_2	ξ_3	ξ_4	Effects on the GCI	Type	Interpretations on δx
0	0	0	GCI $\downarrow$ as $\xi_1 \uparrow$	FP	Electrical noises or spikes of unconnected neurons.
$-$	$-$	$-$	GCI $\downarrow$ as $\xi_1 \uparrow$	FN	Spike missing.
0	$+$	$+$	GCI $\uparrow$ as $\xi_3 \uparrow$ or $\xi_4 \uparrow$	FP	Connected neurons which are positively correlated with the target neuron.
$+$	$+$	$+$	GCI $\uparrow$ if (ξ_3, ξ_4) dominates ξ_2 GCI $\downarrow$ if ξ_2 dominates (ξ_3, ξ_4)	FP	Connected neurons which are positively correlated with both of source and target neurons.

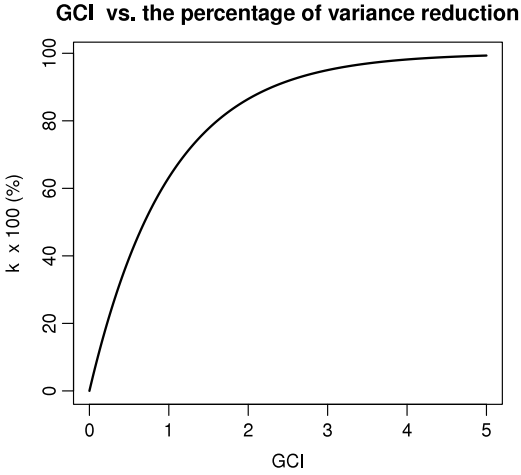

Fig. 1. The relationship between the Granger Causality Index (GCI) and k. This transforms GCI values to the corresponding percentage of variance reduction in the residual noise process.

Spike sorting errors include two types: fake (FP) and missing (FN) spike events. The fake spike event is an erroneous detection of an event that is not a real spike or is a spike from another neuron. Conversely, a missing spike event means that spikes were not detected or were classified into groups of other neurons. Therefore, the fake spike case can be regarded as adding extra points to a point process. This type of error is denoted by "A-type". The missing spike case can be regarded as removing some points from a point process, and is denoted by "R-type". Forms of the addition or removal of points are considered for uniform, random, and concentrative distributions. The number of fake or missing spike events is rN, where r ($=p\%$) is the ratio of fake or missing points compared to the original spike train. The following explains the generation of these types in detail.

Uniform-partition addition (PA) model: The extra points $\{\tilde{p}_i : 1 \le i \le rN\}$ on the time interval $[0, T]$ form a uniform partition of $[0, T]$. More precisely, $\tilde{p}_i = i\Delta t$, where $\Delta t = \frac{T}{rN-1}$.
Random-uniform addition (UA) model: The extra points $\tilde{p}_i$, $i = 1, \ldots, rN$, on the time interval are generated from a uniform distribution $\mathcal{U}([0, T])$ random variable.
Random-normal addition (NA) model: The extra points $\tilde{p}_i$, $i = 1, \ldots, rN$, on the time interval are generated from a normal distribution $\mathcal{N}(T/2, \sigma_{\mathrm{NA}})$ random variable. The standard deviation parameter σ_{NA} represents different degrees of concentration.
Uniform-partition removal (PR) model: A set of reference points $\{\tilde{p}_j : 1 \le j \le rN\}$, which is a uniform partition of $[0, T]$ was used to remove spike events from $\{p_i : 1 \le i \le N\}$. First, fix $\tilde{p}_j$ and then remove the point that is closest to $\tilde{p}_j$.
Random-uniform removal (UR) model: Points in $\{p_i : 1 \le i \le N\}$ are randomly removed using a discrete uniform $\mathcal{U}_d(1, N)$ random variable, i.e., all points have the same probability of being removed.
Middle-succession removal (SR) model: In this model, the removed points are successive and located near the center $T/2$ of the time interval $[0, T]$. The number of spikes is rN.

We note that sorting errors only occur in the source process X, and Y is assumed to be inerrable.

3.2. Setup

Set the parameters, $\lambda = 2$, $T = 100$, $m = 0.1$ for the rate of the Poisson process, the total time, and the time lag, respectively. To apply autoregressive modeling, we convert point processes $\{p_i : 1 \le i \le N\}$ and $\{q_i : 1 \le i \le N\}$ to time series through the procedure of binning with the bin size as the time lag m. Results are obtained from the average of 100 simulations for each random case at fixed error percentage r. To investigate the effects of errors on the GCI, we observe the results from various r, σ, and σ_{NA}.

3.3. Simulation results

We note that the simulations and the corresponding results are related to Corollaries 1–3 of Section 2.3.

3.3.1. A-type vs. R-type

Fig. 2(a) shows the results for experiment 1 in which $\sigma = 0.02$, $\sigma_{\mathrm{NA}} = T/8$, and the error percentage increased by 0.1. In this figure, the GCI of the SR model decreases the fastest among all of the models as r increases. All R-type errors cause information loss and greatly weaken the GCI when the error percentage increases. If $r = 1$, the underlying signal is totally destroyed by the errors, and the causality is undetermined. The PA model produces the largest GCI for a fixed r. Fig. 2(a) also shows that A-Type GCIs are greater than R-Type GCIs. However, this phenomenon is not always valid. The error in the NA model is uncorrelated with the signal and weakens the GCI more than any of the R-Type models when σ_{NA} is small. Fig. 2(b) shows that a highly non-stationary process can average out much more underlying causality than the others, for the case of $\sigma_{\mathrm{NA}} = T/64$ in the NA model.

3.3.2. Standard deviation factor σ

We now investigate the effects of the standard deviation σ on GCIs. Fig. 2(c) and (d) show the results for experiments 2 and 3 in which parameter σ is 0.04 and 0.06, respectively. Observations in Fig. 2(a), (c), and (d) show that the behaviors of the profiles with $\sigma = 0.04, 0.06$ closely resemble the behavior of the profile with $\sigma = 0.02$. In the PA and PR models, let F denote the GCI value without a sorting error ($r = 0$), and $\tilde{F}(r)$ denote the GCI value with sorting error of error percentage r. Table 2 presents the relative errors of the GCI for r from 0.1 to 0.9 of the PA and PR models in the three experiments, where

$$\text{Relative error}(r) := \frac{\tilde{F}(r) - F}{F} \times 100\%.$$

Table 2 shows that Experiment 3 had the flattest PA-curve and PR-curve of the three experiments, and the underlying causality of the PA models were all around 50% off at $r = 0.9$ because the signal to noise ratio $\left(SNR = \frac{\mathrm{Var}(x)}{\mathrm{Var}(\delta x)}\right)$ was close to 1. Although they were all around 50% off, the corresponding decreases in the percentage of variance reduction are greatly differed, and this can be seen from

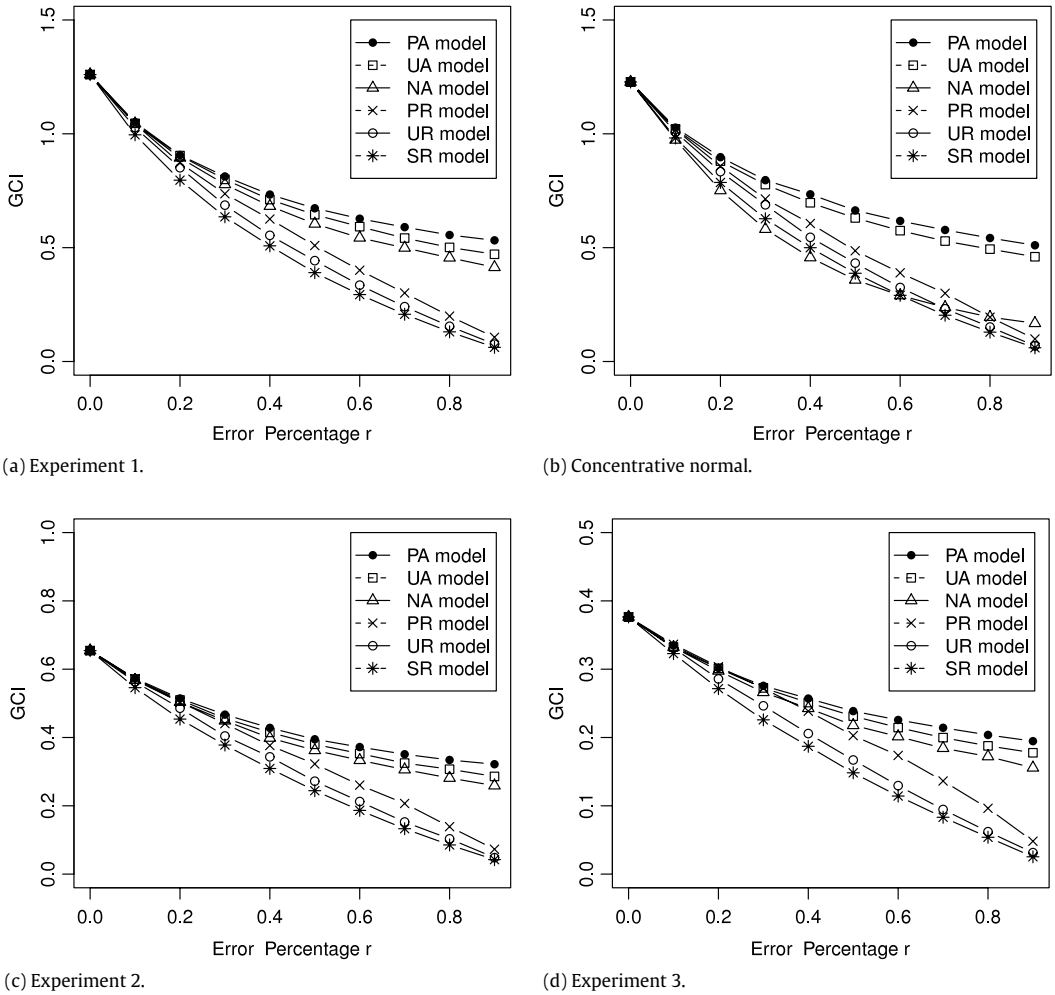

(a) Experiment 1.

(b) Concentrative normal.

(c) Experiment 2.

(d) Experiment 3.

Fig. 2. (a) Simulation results of Experiment 1, in which the parameter settings were $\lambda = 2$, $T = 100$, $m = 0.1$, $\sigma = 0.02$. (b) Simulation results of a much more concentrative normal, in which the parameter settings were $\lambda = 2$, $T = 100$, $m = 0.1$, $\sigma = 0.02$, and $\sigma_{NA} = T/64$. (c) Simulation results of Experiment 2, in which the parameter settings were $\lambda = 2$, $T = 100$, $m = 0.1$, $\sigma = 0.04$. (d) Simulation results of Experiment 3, in which the parameter settings were $\lambda = 2$, $T = 100$, $m = 0.1$, $\sigma = 0.06$. The error percentages r were all 0–0.9, and increased by 0.1.

Table 2

Relative errors, $\frac{\tilde{F}(r)-F}{F} \times 100\%$, of GCI for $r = 0.1$–0.9 of the PA and PR models in the three experiments.

Experiment	$r = 0.1$	$r = 0.2$	$r = 0.3$	$r = 0.4$	$r = 0.5$	$r = 0.6$	$r = 0.7$	$r = 0.8$	$r = 0.9$
Relative errors (%) of the PA model									
$1(\sigma = 0.02)$	−16.46	−27.24	−35.29	−41.48	−46.26	−50.26	−53.43	−55.78	−57.60
$2(\sigma = 0.04)$	−12.27	−21.87	−29.41	−34.36	−39.84	−42.63	−46.28	−48.93	−51.20
$3(\sigma = 0.06)$	−11.59	−19.78	−26.99	−32.13	−36.63	−40.89	−43.42	−46.29	−48.41
Relative errors (%) of the PR model									
$1(\sigma = 0.02)$	−17.10	−30.16	−41.89	−51.31	−59.78	−68.60	−75.86	−84.02	−92.07
$2(\sigma = 0.04)$	−12.64	−22.71	−32.74	−41.82	−50.63	−59.24	−68.72	−78.04	−88.96
$3(\sigma = 0.06)$	−11.58	−19.21	−27.60	−37.45	−47.44	−54.15	−65.07	−75.34	−87.68

Fig. 1. In the PA model, the three F values corresponding to the three experiments were 1.24, 0.64, and 0.38, and the corresponding $\tilde{F}(0.9)$ were 0.71, 0.33, and 0.18, respectively. Eq. (14) can compute the corresponding relative decreases in the percentage of variance reduction, which were 28.17%, 40.89%, and 46.85%, respectively.

3.3.3. Explanation of the GCI curves

We now discuss the behaviors of the curves in Fig. 2(a). Because A-type error processes (δx) are uncorrelated with the underlying process (x), curves of the PA, UA, and NA models can be analyzed and directly explained by (6) and (10). These three curves decrease as the size of the errors (ξ_1) increases. They reach zero only when the error size is infinity, which is actually unfeasible. Therefore, these curves slowly decrease and never reach zero. In other words, the underlying causality remains.

Moreover, the PA-curve is above the UA-curve, and the UA-curve is above the NA-curve. This is because the NA model has the largest error size, followed by the UA model and the PA model at the same error percentage. On the other hand, error processes of the PR, UR, and SR models are correlated with the underlying process, and (12) is used instead of (10) since ξ_2, ξ_3, and ξ_4 are nonzero.

With approximately the same error size, these curves decrease much more quickly than the uncorrelated case because of the

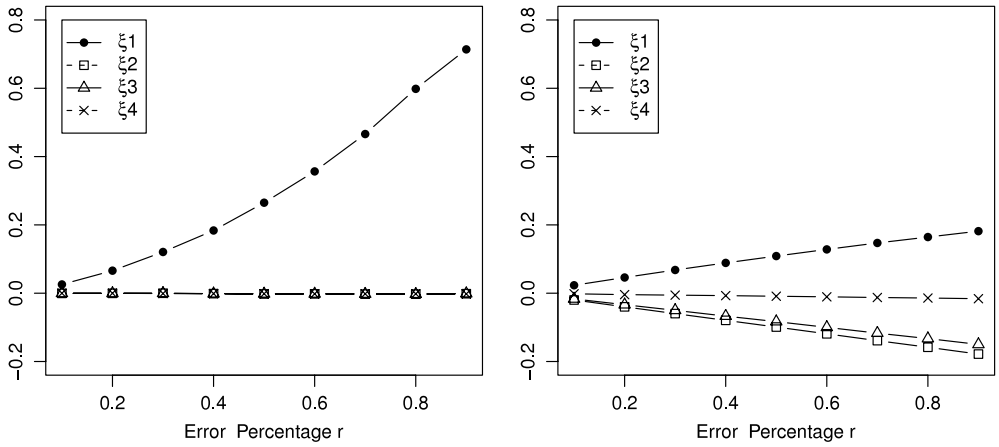

(a) The ξ_1 to ξ_4 of NA model. (b) The ξ_1 to ξ_4 of SR model.

Fig. 3. (a) ξ_1 to ξ_4 of the NA model, in which the parameter settings were $\lambda = 2, T = 100, m = 0.1, \sigma = 0.02, \sigma_{NA} = T/64$. (b) ξ_1 to ξ_4 of the SR model, in which the parameter settings were $\lambda = 2, T = 100, m = 0.1, \sigma = 0.02$. The error percentages r were both 0–0.9, and increased by 0.1.

negative correlations. Unlike the former, these curves almost reach zero at the error percentage $r = 0.9$. In addition, the PR-curve is above the UR-curve, and the UR-curve is above the SR-curve. This is because the SR model has the largest error size, followed by the UR and PR models at the same error percentage.

We now discuss the behaviors of the curves in Fig. 2(b), which shows that A-type errors are not always better than R-type errors. GCI values of the NA model with $\sigma_{NA} = T/64$ are smaller than those of the SR model when the error percentage is between $r = 0.2$ and $r = 0.6$. To see what occurred, we computed ξ_1 to ξ_4 at each error percentage for these two cases, and results are respectively shown in Fig. 3(a) and (b). Comparing these two panels indicates that (i) ξ_1 of the NA model is much larger than that of the SR model. According to (12), the GCI of the NA model is smaller than that of the SR model. (ii) The SR model has large ξ_2 and ξ_3. According to (13), the GCI of the SR model is significantly smaller than that of the NA model when r is quite large, even though the ξ_1 of the SR model is still relatively smaller than that of the NA model. Fig. 2(b) verifies this analysis showing that the error size of the NA model dominates the negative correlation of the SR model when the error percentage is between $r = 0.2$ and $r = 0.6$. Contrarily, the negative correlation of the SR model dominates the error size of the NA model when $r > 0.6$. Therefore, it is necessary to integrate the error size and the negative correlation to identify the behavior of the GCI, and the reason is that the error size of the NA model is much larger than that of the SR model when $0 \leq r \leq 0.6$.

3.4. Supplementary simulations of FPs

We now present supplementary simulations of FPs by considering the case when FPs are composed of connected neurons. There are no supplementary simulations for FNs since they have only one situation as discussed in Corollary 2, and they were simulated in preceding work. The simulations here are devoted to Corollaries 4 and 5 of Section 2.3. The following explain the simulations in detail and the model parameters are fixed at $\lambda = 2, T = 100, m = 0.1$, and $\sigma = 0.02$.

Experiment A: Suppose X and Z are two independent Poisson processes with equal rate λ in $[0, T]$, where N is the total number of points of X. Let Y be another point process generated by $Y = Z + \mathcal{N}(m, \sigma)$. Hence, we have that Y is induced by Z, and X is independent of both Y and Z. Then rN points of Z are randomly added to X, where r denotes the error percentage. After binning with bin size m, the GCI from X to Y as a function of r and the corresponding ξ's are shown in Fig. 4(a) and (b). This experiment considers the situation that FPs are composed of spikes of connected neurons which are positively correlated with target neurons. Note that the true causality between X and Y is uncorrelated (GCI = 0), which means that the relationship between neurons may be erroneously identified when a FP occurs during spike sorting.

Experiment B: Here we consider another situation that Y is induced by both X and Z, that is, $Y = \{X + \mathcal{N}(m, \sigma)\} \cup \{Z + \mathcal{N}(m, \sigma)\}$, where X and Z are independent Poisson processes with equal rate λ in $[0, T]$. Then rN points of Z are randomly added to X. After binning, the GCI from X to Y and the corresponding ξ's are shown in Fig. 4(a) and (c). The result shows that the relationship is correctly identified, but the strength (GCI) is overestimated. Experiments A and B enlighten that the risk of an erroneous causal identification should be estimated by two parts: the relationship (causal or noncausal) and the strength (the magnitude of the GCI).

Experiment C: Suppose Z is a Poisson processes with rate λ in $[0, T]$. Let X and Y be point processes generated by $X = Z + \mathcal{N}(m, \sigma)$ and $Y = X + \mathcal{N}(m, \sigma)$, i.e., X is induced by Z, and Y is induced by X. Then rN points of Z are randomly added to X. After binning, the GCI from X to Y and the corresponding ξ's are shown in Fig. 4(a) and (d). The result shows that the effect of the positive-correlation ($\xi_2 > 0$) between Z and X dominates the effect of the positive-correlation ($\xi_3 > 0, \xi_4 > 0$) between Z and Y; thus the GCI decreases. This experiment is devoted to Corollary 5 of Section 2.3.

3.5. Simulation for threshold detection

Spike sorting consists of two parts: AP detection and AP classification, which are based on thresholding and clustering methods, respectively. Here we discuss the relationship between the GCI value and the detecting threshold via simulation. The classification part will be discussed in Section 4 by using real experimental data.

We simulate a sequence of 100 APs, denoted by $\mathcal{A}$, having fixed interspike interval (ISI) length as shown in Fig. 5(a). Then we add an independent white noise to $\mathcal{A}$ with $SNR = 0.8$ for the background noise. Denoting the standard deviation of the observed noisy data by τ, Fig. 5(b) and (c) show the detected spikes with threshold values being 2.5τ and 3.0τ, respectively. It is easy to see that a lower threshold is tending to result in FPs of spike-detection and a higher one is tending to result in FNs. Now, let pX be the point process obtained from perfect-detection, i.e., pX coincides with $\mathcal{A}$. Let $pY = pX + \mathcal{N}(0.1, 0.02)$ represent the point process

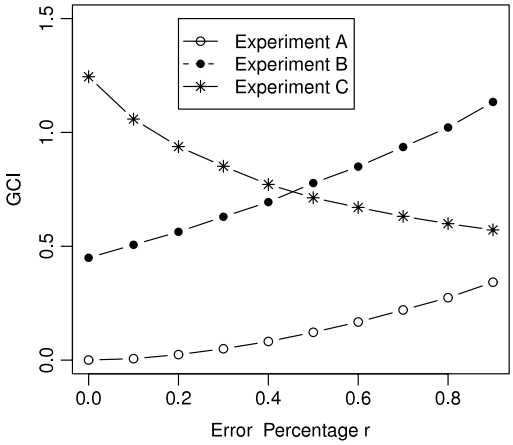

(a) Supplementary simulations for FP.

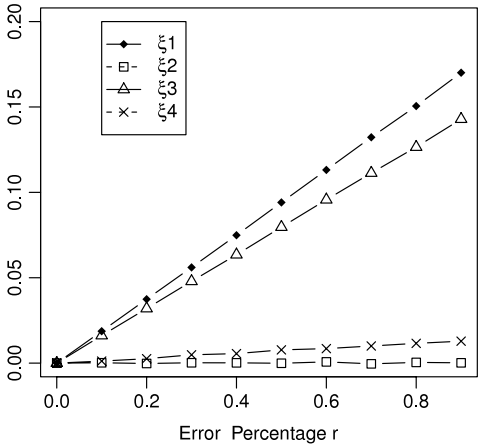

(b) The ξ_1 to ξ_4 of Experiment A.

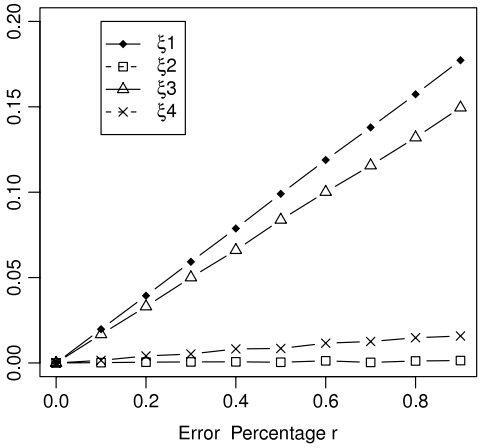

(c) The ξ_1 to ξ_4 of Experiment B.

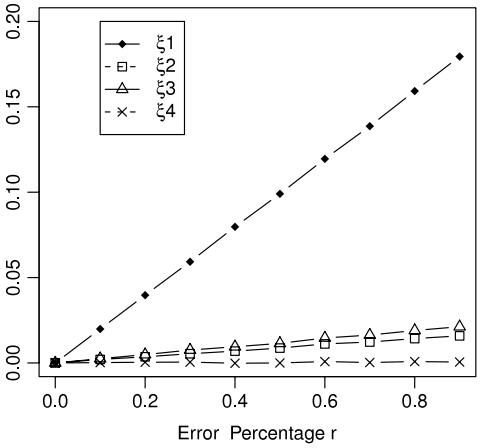

(d) The ξ_1 to ξ_4 of Experiment C.

Fig. 4. (a) Simulation results of Experiment A–C for FP. (b) ξ_1 to ξ_4 of the Experiment A. (c) ξ_1 to ξ_4 of the Experiment B. (d) ξ_1 to ξ_4 of the Experiment C.

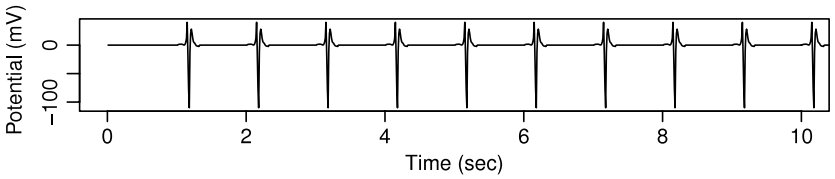

(a) Underlying action potentials.

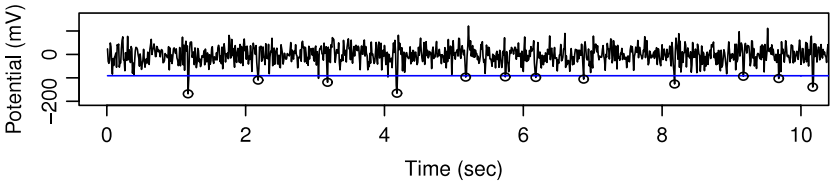

(b) Spike-detection with threshold value 2.5 s.d.

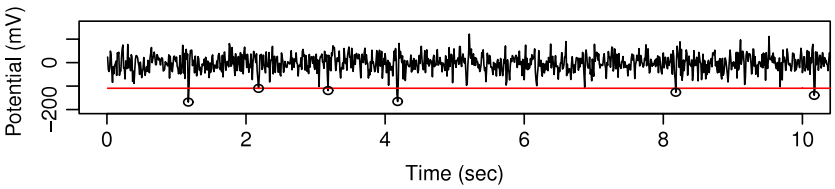

(c) Spike-detection with threshold value 3 s.d.

Fig. 5. (a) The first 10 APs of the underlying AP sequence $\mathcal{A}$. (b) The detected spikes (marked by ○) with threshold value 2.5τ. (c) The detected spikes (marked by ○) with threshold value 3.0τ.

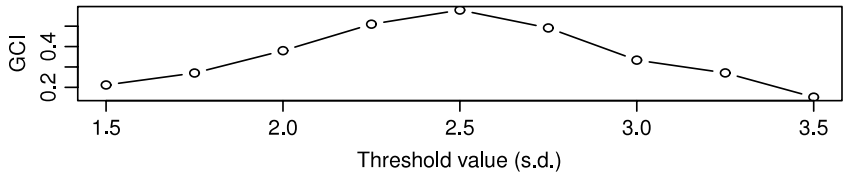

(a) GCI result with varying threshold values.

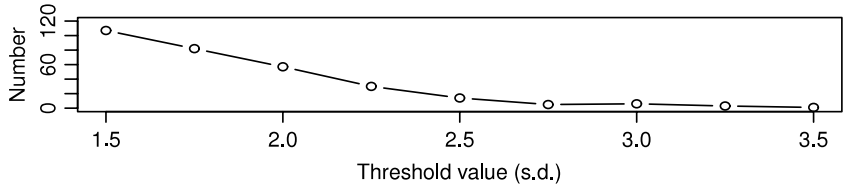

(b) Number of false positives.

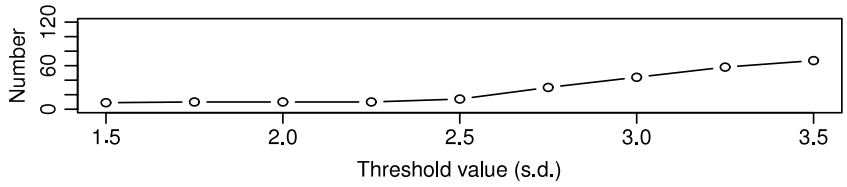

(c) Number of false negatives.

Fig. 6. (a) The relationship between GCI value and threshold value by changing the threshold from 1.5τ to 3.5τ. (b) Number of FPs increases as threshold value decreases. (c) Number of FNs increases as threshold value increases.

obtained from a causal sequence of APs, say $\mathcal{B}$. After binning with bin width 0.1, we can infer the causal relationship between these two sequences of APs, $\mathcal{A}$ and $\mathcal{B}$, by computing the GCI from the binned data of pX to that of pY. To be consistent with our analyses, the errors created by threshold-detection will be put only on the source sequence $\mathcal{A}$. We are now ready to investigate the relationship between GCI value and threshold value by changing the threshold from 1.5τ to 3.5τ, and it is shown in Fig. 6(a). The result shows that 2.5τ performs the best (i.e., obtaining the largest GCI value), since we know that $\mathcal{B}$ is induced by $\mathcal{A}$. To investigate more deeply into this result, numbers of FPs and FNs are further shown in Fig. 6(b) and (c), and these results give us the following findings: (i) Number of FPs increases as threshold value decreases. (ii) Number of FNs increases as threshold value increases. (iii) FPs affect GCI less than FNs since the number of FPs (>100 at 1.5τ) is much larger than that of FNs (>60 at 3.5τ) and the decreasing rate (slope) of GCI in [2.5, 3.5] (=0.4270) is larger than the increasing rate (slope) of GCI in [1.5, 2.5] (=0.3674). (iv) As a result of (iii), we can conclude that choosing a threshold lower than the optimal ($=2.5\tau$) is better and preserves more information than choosing a threshold higher than the optimal.

We now discuss in details the result of this simulation through the following four remarks: (1) For a large threshold, the sorting error is only composed of FNs, without FPs. Therefore the GCI increases as threshold decreases. When the threshold decreases to certain value, the error of FPs occurs. The GCI will reach the maximum and then decreases as the threshold decreases to 0. This result contributes the explanation of the effects of FPs and FNs on the GCI. (2) We can conclude that variations of the GCI are determined by which one of FP and FN to be the dominate sorting error and the total number of FPs and FNs as well for a fixed threshold. (3) Although we cannot choose the optimal threshold in real experiments, (iv) is still useful and it gives a criterion for designing methods of choice of an optimal threshold. (4) Researchers may imitate the procedure of the simulation by using their own $\mathcal{A}$ and background noise to determine the optimal threshold after examining the number of FPs and FNs.

4. Real data evaluation

Here we design two sorting procedures in real operation and then evaluate the effect of sorting errors on the GCI using real experimental data.

4.1. Experimental setup

Neuronal spikes were recorded from the ventroposterior medial (VPM) nucleus of the thalamus and are the same data set used in our previous study (Tseng, Tsai, Iwata, & Yen, 2012). The single-unit recording method is described in Tseng's report (2012). Briefly, spikes were amplified (7000 32,000-fold), filtered (0.25 13 kHz), and digitized at 40 kHz. Recording was performed while a rat was awake. Extracellular single units were recorded in real time using time-voltage windows and a principle component-based template-matching algorithm (Sort Client, Plexon). Waveforms were saved and re-sorted using Offline Sorter (Plexon), based on principle-component clustering, with a user-defined template. The sample we used here contained 2 or more distinguishable clusters. To evaluate the effect of sorting errors on the GCI, various percentage errors were created from 20%, 40%, 60%, and 80% less or more than the data set of a complete cluster. Shrinkage or expansion of the sample size was calculated based on the difference between a waveform of a neuron and a template, computed by the Offline Sorter (tolerance fit function). Note that cluster expansion included the other cluster of a neuron or noises. We used 6 neurons with an averaged firing frequency of 0.199 Hz, and therefore $\binom{6}{2} \times 2 = 30$ neuron pairs (i.e., GCIs) were derived ($(\text{Neuron}^i, \text{Neuron}^j)$ $i = 1, \ldots, 6$ $j \neq i$). Being consistent with our analyses, the errors created by shrinkage or expansion were put only on the source (Neuron^i). In the sequel, we use the FN and FP-procedures to respectively represent shrinkage and expansion operations.

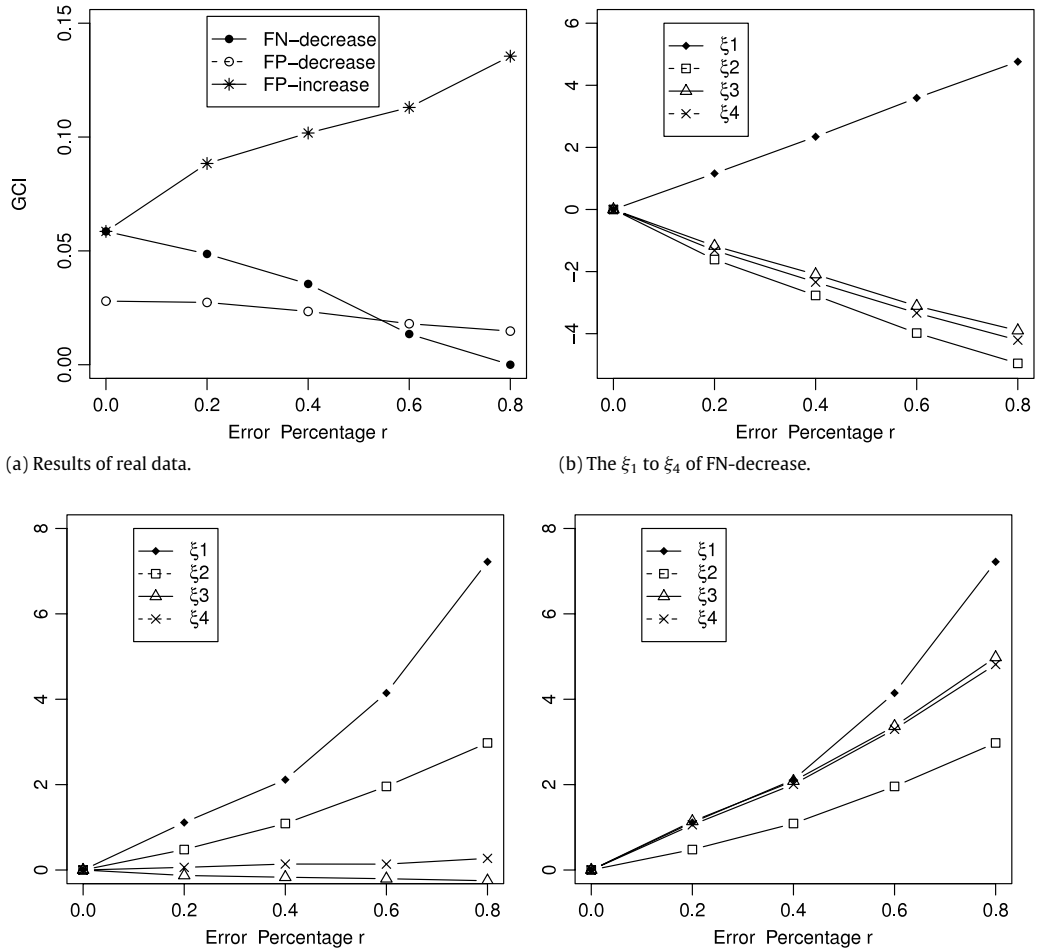

(a) Results of real data.

(b) The ξ_1 to ξ_4 of FN-decrease.

(c) The ξ_1 to ξ_4 of FP-decrease.

(d) The ξ_1 to ξ_4 of FP-increase.

Fig. 7. (a) Three kinds of Granger Causality Index (GCI) patterns which frequently appeared in real experimental data. (b) ξ_1 to ξ_4 of the false-negative (FN)-decrease pattern. (c) ξ_1 to ξ_4 of the false-positive (FP)-decrease pattern. (d) ξ_1 to ξ_4 of the FP-increase pattern.

4.2. Experimental results

From these real data we found three GCI patterns which frequently appeared under the above-mentioned sorting procedures, one of them was found under the FN-procedure, and the other two were found under the FP-procedure. These patterns are explained in detail.

FN-decrease: The GCIs of all the neuron pairs (24 of 30 pairs) decreased as the error percentage increased under the FN-procedure (Fig. 7(a)) except pairs with a zero GCI (6 of 30 pairs). The four corresponding ξ's are shown in Fig. 7(b), and it shows that the error process induced by the FN-procedure was negatively correlated with processes of both the source and target neurons; thus the GCI decreased (resembling that in Fig. 3(b)).

FP-decrease: The GCIs of neuron pairs (6 of 30 pairs) decreased as the error percentage increased under the FP-procedure (Fig. 7(a)) and the four corresponding ξ's of this pattern (Fig. 7(c)) show that the error process was positively correlated with process of the source neuron and was uncorrelated with that of the target neuron. The GCI decreased because the effect of ξ_2 dominated the effect of ξ_3 and ξ_4. In other words, the error process was composed of spikes of some connected neurons which were positively correlated with the source neuron.

FP-increase: The GCIs of neuron pairs (16 of 30 pairs) increased as the error percentage increased under the FP-procedure (Fig. 7(a)) and the four corresponding ξ's of this pattern (Fig. 7(d)) show that the error process was positively correlated with processes of both the source and target neurons. The GCI increased because the effect of ξ_3 and ξ_4 dominated the effect of ξ_2. In other words, the error process was composed of spikes of some connected neurons which were strongly correlated with the target neuron.

Finally, we note that there are 5 neuron pairs with a zero GCI, and 3 neuron pairs with unchanged GCIs under the FP-procedure.

5. Discussion

Because spike sorting errors are almost unavoidable, this study was devoted to investigating how sorting errors affect the identification of information flow among neurons. The analyses of this paper allowed us to directly discuss the effects of FPs and FNs through the proposed formula, and the results also revealed that they do not have the same effect on spike sorting. In Section 2, we derived an analytic formula (7) in terms of factors ξ_1 to ξ_4, and this formula can be used, when incorporating (6), to obtain how the GCI changes according to the error signal. Under the FN type of sorting error, we know the error process is negatively correlated with processes of both the source and target neurons; thus the GCI will always be underestimated. On the other hand, under the FP type of sorting error, the GCI may be underestimated or overestimated depending on the error process. If the error process is only composed of electrical noise or spikes of other unconnected

neurons, the GCI will be underestimated, but in general, the accuracy is better than cases of the FN type. If the error process is composed of spikes of some positively correlated neurons, then the GCI will be overestimated, and a noncausal neuron pair may be mistaken for a causal pair.

From the perspective of the GC, we provide some suggestions for spike sorting. (i) Missing successive spikes should be avoided as far as possible since this mostly weakens the GCI (Fig. 2(a), SR model). (ii) A-type errors, which are concentratively added, may weaken the underlying GCI more than R-type errors (Fig. 2(b), NA model). (iii) During spike detection, choosing a threshold lower than the optimal is better than choosing a threshold higher than the optimal because fake spike events (electrical noise) affect the GCI less than missing spike events (Figs. 2(a), (c), (d), and 6). (iv) During spike classification, cluster shrinkage from the optimal cluster is better than cluster expansion from the optimal because FPs may result in overestimating the GCI and mistaking a noncausal neuron pair for a causal pair (Fig. 4(a), Experiment A). FNs can only result in an underestimation of the GCI (Fig. 7(a), FN-decrease), and this is a relatively conservative and secure strategy for scientific research. For (i) and (ii), in fact, we really cannot avoid missing spikes successively or adding spikes concentratively in the analysis of real data. However, our suggestions still are useful in some cases when recordings are made in the brain regions that neurons are known with complementary intermittence discharge. For example, since the inspiratory-related and expiratory-related neurons coexist in the dorsal and ventral respiratory group (Takeda & Matsumoto, 1997), and the firing of these two types of neurons are complementary intermittence, so successive missing or concentrative adding of spikes after sorting may occur. We should examine the time series of spike trains to ensure if the patterns of complementary intermittence are confused after sorting, and to infer which modification would be made when GCIs are calculated. For (iii) and (iv), these two conclusions are just opposite to each other. That is, in spike detection, the FPs are better than the FNs, because the FPs consist of only electrical noises. But in spike classification, the FNs are better than the FPs because the FPs consist of not only electrical noises but also maybe some causal neurons. Finally we note that the way of choosing an optimal threshold or cluster size varies from case to case, since it depends on the sorting method used, and the experimental situation you met. This study is just trying to give a general concept for choosing a better threshold and cluster size.

The results of this study are based on restrictive situations. The analytic formula was obtained from a first order autoregressive model, and the error processes were only superposed on the source process. However, based on these simplifications, the intrinsic properties of the GCI can be seen more clearly than in complete but more complicated situations. Although there are still a lot of concerns on the technical aspect of applying the GCI to determine the relationship among neurons in practice, researchers may be interested in understanding intuitively the effect of spike sorting error before these techniques are really applied, and this is exactly what this paper wants to provide. Real neuronal networks are much more complex than the simplified assumptions of the analyses and simple models of the simulation. The procedures presented in this study need further development to approach the complex reality. The well-established framework of information theory, for example, might be employed to provide more-credible statistical inferences about true causality in the future.

Appendix. Derivation of the explicit formula

We first denote $x_k = x(n-k)$ and $y_k = y(n-k)$ for convenience. Then for the model in (1), we compute matrices $\mathbf{A}$ and $\mathbf{\Sigma}$ by the method of Yule–Walker (Priestley, 1994). Since x and y are stationary, multiply (1) from the right by the vector $\left[x(n-1)\ y(n-1)\right]$ and then take the expectation E, we have $\mathbf{R}(-1) = \mathbf{A}\mathbf{R}(0)$, where

$$\mathbf{R}(0) = \begin{bmatrix} E\left(x_1^2\right) & E\left(x_1y_1\right) \\ E\left(x_1y_1\right) & E\left(y_1^2\right) \end{bmatrix} \quad \text{and}$$

$$\mathbf{R}(-1) = \begin{bmatrix} E\left(x_1x_2\right) & E\left(x_2y_1\right) \\ E\left(x_1y_2\right) & E\left(y_1y_2\right) \end{bmatrix}.$$

Thus, we get $\mathbf{A} = \mathbf{R}(-1)\mathbf{R}^{-1}(0)$. Alternatively, $\mathbf{\Sigma}$ can be obtained by $\mathbf{\Sigma} = \mathbf{R}(0) - \mathbf{A}\mathbf{R}^{\top}(-1)$ (Wei, 2006). Substituting $\mathbf{A}$ into $\mathbf{\Sigma}$ gives

$$\mathbf{\Sigma} = \mathbf{R}(0) - \mathbf{R}(-1)\mathbf{R}^{-1}(0)\mathbf{R}^{\top}(-1). \tag{A.1}$$

Using the same computation, we have $\tilde{\mathbf{A}} = \tilde{\mathbf{R}}(-1)\tilde{\mathbf{R}}^{-1}(0)$ and $\tilde{\mathbf{\Sigma}} = \tilde{\mathbf{R}}(0) - \tilde{\mathbf{A}}\tilde{\mathbf{R}}^{\top}(-1)$ for the perturbed model in (4), where

$$\tilde{\mathbf{R}}(0) = \begin{bmatrix} E\left(x_1^2 + \delta x_1^2 + 2x_1\delta x_1\right) & E\left(x_1y_1 + y_1\delta x_1\right) \\ E\left(x_1y_1 + y_1\delta x_1\right) & E\left(y_1^2\right) \end{bmatrix}$$

and

$$\tilde{\mathbf{R}}(-1) = \begin{bmatrix} E\left((x_1 + \delta x_1)(x_2 + \delta x_2)\right) & E\left(x_2y_1 + y_1\delta x_2\right) \\ E\left(x_1y_2 + y_2\delta x_1\right) & E\left(y_1y_2\right) \end{bmatrix}.$$

Substituting $\tilde{\mathbf{A}}$ into $\tilde{\mathbf{\Sigma}}$ also gives

$$\tilde{\mathbf{\Sigma}} = \tilde{\mathbf{R}}(0) - \tilde{\mathbf{R}}(-1)\tilde{\mathbf{R}}^{-1}(0)\tilde{\mathbf{R}}^{\top}(-1). \tag{A.2}$$

Using (A.1) and (A.2), and denoting $\delta\mathbf{R}(0) := \tilde{\mathbf{R}}(0) - \mathbf{R}(0)$ and $\delta\mathbf{R}(-1) := \tilde{\mathbf{R}}(-1) - \mathbf{R}(-1)$, it follows that

$$\begin{aligned} \mathbf{\Delta} &:= \tilde{\mathbf{\Sigma}} - \mathbf{\Sigma} \\ &= \delta\mathbf{R}(0) - \delta\mathbf{R}(-1)\mathbf{R}^{-1}(0)\mathbf{R}(1) - \tilde{\mathbf{R}}(-1)\mathbf{R}^{-1}(0)\delta\mathbf{R}(1) \\ &\quad + \tilde{\mathbf{R}}(-1)\mathbf{R}^{-1}(0)\delta\mathbf{R}(0)\tilde{\mathbf{R}}^{-1}(0)\tilde{\mathbf{R}}(1). \end{aligned} \tag{A.3}$$

By the definition of S and $\tilde{S}$ defined in (5) we know that $\tilde{S} - S = \mathbf{\Delta}_{2,2}$, the (2, 2)-element of matrix $\mathbf{\Delta}$. Hence, we can decompose $\tilde{S}$ into $S + \mathbf{\Delta}_{2,2}$. Annoying algebraic computation from (A.3) gives $\mathbf{\Delta}_{2,2} = (S_y - S)I$, where I is defined in (7), and the formula in (6) is obtained by denoting $\Theta = (S_y - S)I$.

References

Baccala, L. A., & Sameshima, K. (2001). Partial directed coherence: a new concept in neural structure determination. *Biological Cybernetics*, *84*, 463–474.

Bressler, S. L., Richter, C. G., Chen, Y., & Ding, M. (2007). Cortical functional network organization from autoregressive modeling of local filed potential oscillations. *Statistics in Medicine*, *26*, 3875–3885.

Bressler, S. L., & Seth, A. K. (2011). Wiener–Granger causality: a well established methodology. *NeuroImage*, *58*, 323–329.

Brown, E. N., Kass, R. E., & Mitra, P. P. (2004). Multiple neural spike train data analysis: state-of-the-art and future challenges. *Nature Neuroscience*, *7*, 456–461.

Cadotte, A. J., DeMarse, T. B., He, P., & Ding, M. (2008). Causal measures of structure and plasticity in simulated and living neural networks. *PLoS Computational Biology*, *3*, 1–14.

Cadotte, A. J., DeMarse, T. B., Mareci, T. H., Parekh, M. B., Talathi, S. S., Hwang, D. U., et al. (2010). Granger causality relationships between local field potentials in an animal model of temporal lobe epilepsy. *Journal of Neuroscience Methods*, *189*, 121–129.

Cao, Y., Maran, S. K., Dhamala, M., Jaeger, D., & Heck, D. H. (2012). Behavior-related pauses in simple-spike activity of mouse purkinje cells are linked to spike rate modulation. *Journal of Neuroscience*, *25*, 8678–8685.

Deborah, S., Won, D. Y., & Patrick, D. W. (2003). Effects of spike sorting error on information content in multi-neuron recordings. In *Proceedings of the 1st international IEEE EMBS conference on neural engineering, 3* (pp. 618–621).

Dhamala, M., Rangarajan, G., & Ding, M. (2008). Analyzing information flow in brain networks with nonparametric Granger causality. *NeuroImage*, *41*, 354–362.

Ding, M., Chen, Y., & Bressler, S. L. (2006). Granger causality: basic theory and application to neuroscience. In *Handbook of time series analysis: recent theoretical developments and applications* (pp. 437–460). Weinheim, Germany: Wiley-VCH Verlag GmbH & Co. KGaA.

Granger, C. (1969). Investigating causal relations by econometric models and cross-spectral methods. *Econometrica*, *37*, 424–438.
Granger, C. (1980). Testing for causality: a personal viewpoint. *Journal of Economic Dynamics and Control*, *2*, 329–352.
Kaminski, M., Ding, M., Truccolo, W. A., & Bressler, S. L. (2001). Evaluating causal relations in neural systems: Granger causality, directed transfer function and statistical assessment of significance. *Biological Cybernetics*, *85*, 145–157.
Kim, S., Putrino, D., Ghosh, S., & Brown, E. N. (2011). A Granger causality measure for point process models of ensemble neural spiking activity. *PLoS Computational Biology*, *7*(3).
Lewicki, M. S. (1998). A review of methods for spike sorting: the detection and classification of neural action potentials. *Network: Computation in Neural Systems*, *9*, R53–R78.
Priestley, M. B. (1994). *Spectral analysis and time series*. London: Academic Press.
Takeda, M., & Matsumoto, S. (1997). Discharge patterns of dorsal and ventral respiratory group neurons during spontaneous augmented breaths observed in pentobarbital anesthetized rats. *Brain Research*, *749*(1), 95–100.
Tseng, W. T., Tsai, M. L., Iwata, K., & Yen, C. T. (2012). Long-term changes in trigeminal ganglionic and thalamic neuronal activities following inferior alveolar nerve transection in behaving rats. *Journal of Neuroscience*, *32*, 16051–16063.
Wei, William W. S. (2006). *Time series analysis: univariate and multivariate methods* (2nd ed.) (pp. 391–392). California: Addison-Wesley.
Wiener, N. (1956). The theory of prediction. In *Modern mathematics for engineers, vol. 1*. New York: McGraw-Hill.
Zhang, L., Chen, G., Niu, R., Wei, W., Ma, X., Xu, J., et al. (2012). Hippocampal theta-driving cells revealed by Granger causality. *Hippocampus*, *8*, 1781–1793.
Zhu, L., Lai, Y. C., Hoppensteadt, F. C., & He, J. (2003). Probing changes in neural interaction during adaptation. *Neural Computation*, *15*, 2359–2377.